Integrating Models and Observations: Reducing Biases in Earth System Models and Community Benchmarking of Land Models

Forrest M. Hoffman[1], James T. Randerson[2], William J. Riley[3], Gretchen Keppel-Aleks[4], David M. Lawrence[5], Nathan Collier[1], Jitendra Kumar[1], and William W. Hargrove[6]

[1]Oak Ridge National Laboratory, [2]University of California Irvine, [3]Lawrence Berkeley National Laboratory, [4]University of Michigan Ann Arbor, [5]National Center for Atmospheric Research, and [6]USDA Forest Service

Workshop on Sustained Observations for Carbon Cycle Science and Decision Support
NOAA Earth System Research Laboratory, Boulder, Colorado, USA
April 13–14, 2016

CLIMATE CHANGE SCIENCE INSTITUTE
OAK RIDGE NATIONAL LABORATORY

OAK RIDGE National Laboratory

Research Questions

Question 1

How well do Earth System Models (ESMs) simulate the observed distribution of anthropogenic carbon in atmosphere, ocean, and land reservoirs?

Research Questions

Question 1

How well do Earth System Models (ESMs) simulate the observed distribution of anthropogenic carbon in atmosphere, ocean, and land reservoirs?

Question 2

Can contemporary atmospheric CO_2 observations be used to constrain future CO_2 projections?

Research Questions

Question 1

How well do Earth System Models (ESMs) simulate the observed distribution of anthropogenic carbon in atmosphere, ocean, and land reservoirs?

Question 2

Can contemporary atmospheric CO_2 observations be used to constrain future CO_2 projections?

Community Model Benchmarking

Systematic assessment of model fidelity, employing best-available observational data, can identify model weaknesses and inspire new measurements.

Observed Carbon Accumulation Since 1850

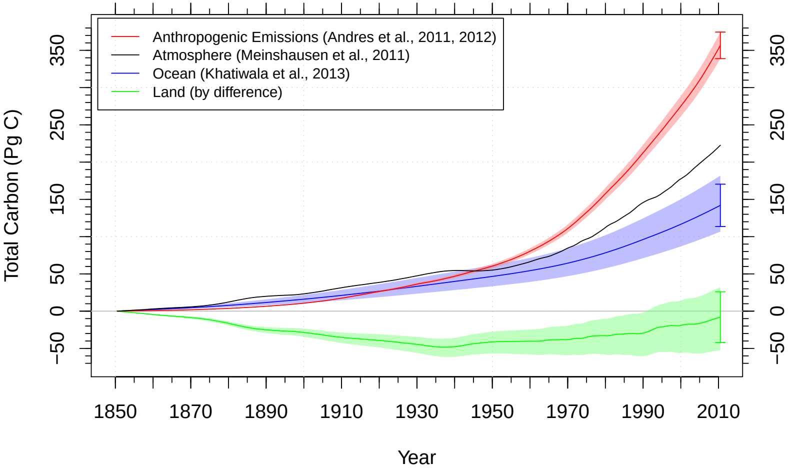

Observational estimates of anthropogenic carbon emissions (excluding land use change) and accumulation in atmosphere, ocean, and land reservoirs for 1850–2010. Atmosphere carbon is a fusion of Law Dome ice core CO_2 observations, the Keeling Mauna Loa record, and more recently the NOAA GMD global surface average, integrated for the purpose of forcing IPCC models. Total land flux is computed by mass balance as follows:

$$\Delta C_L = \sum_i F_i - \Delta C_A - \Delta C_O.$$

15 fully-prognostic ESMs that performed CMIP5 emissions-forced simulations

Model	Modeling Center
BCC-CSM1.1	Beijing Climate Center, China Meteorological Administration, CHINA
BCC-CSM1.1(m)	Beijing Climate Center, China Meteorological Administration, CHINA
BNU-ESM	Beijing Normal University, CHINA
CanESM2	Canadian Centre for Climate Modelling and Analysis, CANADA
CESM1-BGC	Community Earth System Model Contributors, NSF-DOE-NCAR, USA
FGOALS-s2.0	LASG, Institute of Atmospheric Physics, CAS, CHINA
GFDL-ESM2g	NOAA Geophysical Fluid Dynamics Laboratory, USA
GFDL-ESM2m	NOAA Geophysical Fluid Dynamics Laboratory, USA
HadGEM2-ES	Met Office Hadley Centre, UNITED KINGDOM
INM-CM4	Institute for Numerical Mathematics, RUSSIA
IPSL-CM5A-LR	Institut Pierre-Simon Laplace, FRANCE
MIROC-ESM	Japan Agency for Marine-Earth Science and Technology, Atmosphere and Ocean Research Institute (University of Tokyo), and National Institute for Environmental Studies, JAPAN
MPI-ESM-LR	Max Planck Institute for Meteorology, GERMANY
MRI-ESM1	Meteorological Research Institute, JAPAN
NorESM1-ME	Norwegian Climate Centre, NORWAY

CMIP5 Long-Term Experiments

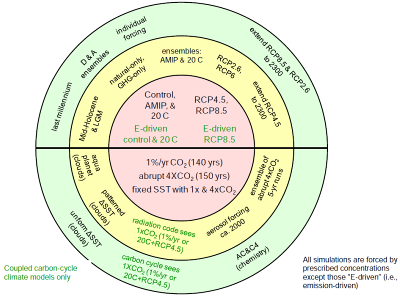

Emissions for Historical + RCP 8.5 Simulations

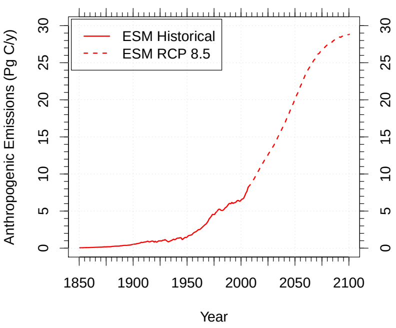

(a) Most ESMs exhibited a high bias in predicted atmospheric CO_2 mole fraction, which ranged from 357–405 ppm at the end of the historical period (1850–2005).

(b) The multi-model mean was biased high from 1946 throughout the 20th century, ending 5.6 ppm above the observed value of 378.8 ppm in 2005.

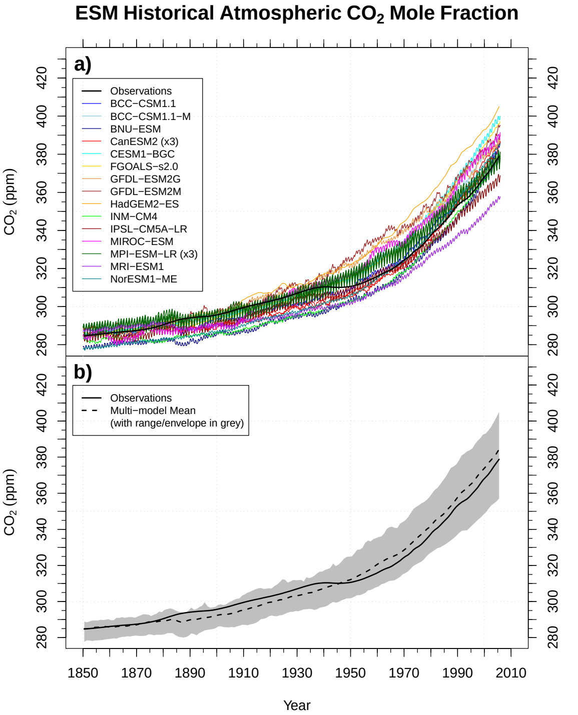

Model inventory comparison with Khatiwala et al. (2013)

Once normalized by their atmospheric carbon inventories, most ESMs exhibited a low bias in anthropogenic ocean carbon accumulation through 2010.

The same pattern holds for the Sabine et al. (2004) inventory derived using the ΔC^* separation technique.

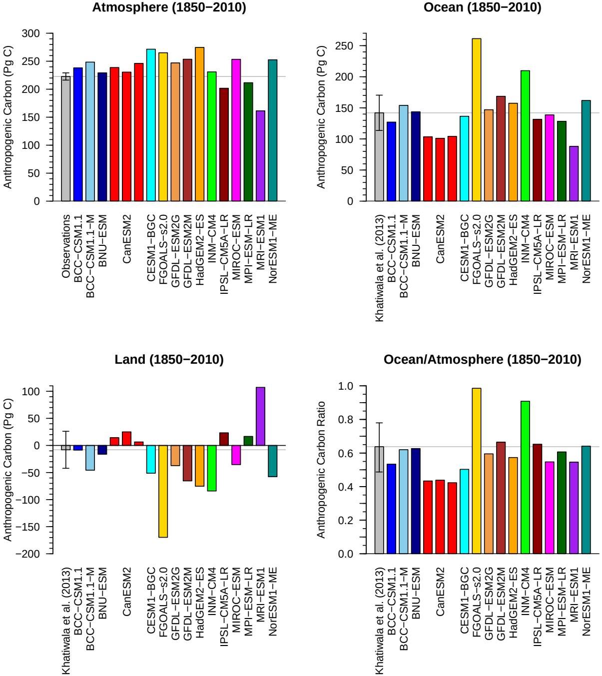

(a) Ocean inventory estimates had a fairly persistent ordering during the second half of the 20th century.

(b) ESMs exhibited a wide range of land carbon accumulation responses to increasing CO_2 and land use change, ranging from a net source of 170 Pg C to a sink of 107 Pg C in 2010.

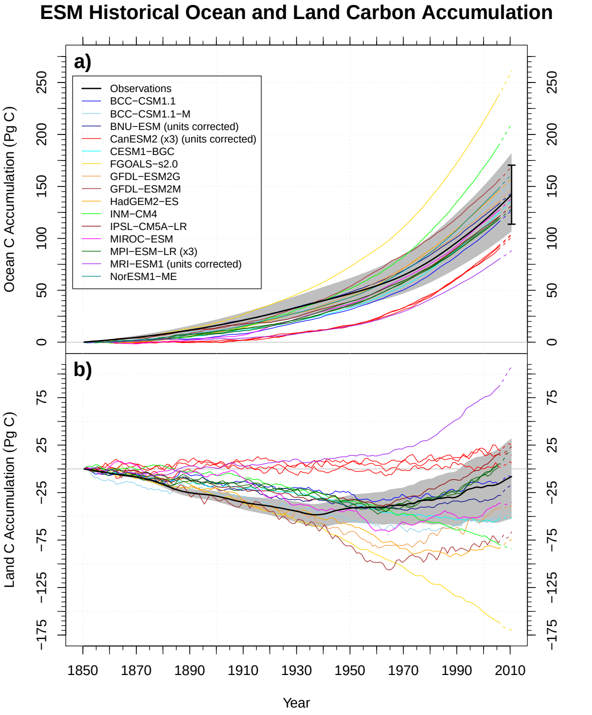

Question 1

How well do Earth System Models (ESMs) simulate the observed distribution of anthropogenic carbon in atmosphere, ocean, and land reservoirs?

- Most ESMs exhibited a high bias in predicted atmospheric CO_2 mole fraction, ranging from 357–405 ppm in 2005.
- The multi-model mean atmospheric CO_2 mole fraction was biased high from 1946 onward, ending 5.6 ppm above observations in 2005.
- Once normalized by atmospheric carbon accumulation, most ESMs exhibited a low bias in ocean accumulation in 2010.
- ESMs predicted a wide range of land carbon accumulation in response to increasing CO_2 and land use change, ranging from -170–107 Pg C in 2010.

Question 2

Can contemporary atmospheric CO_2 observations be used to constrain future CO_2 projections?

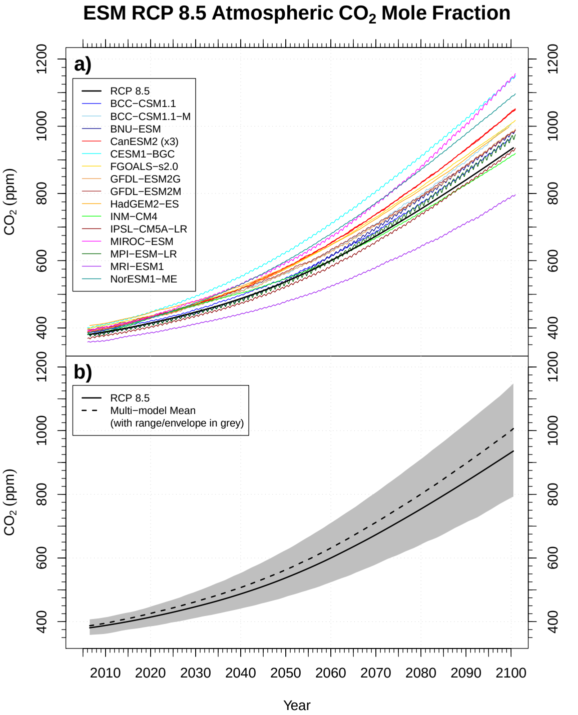

Reducing Uncertainties Using Observations

To reduce feedback uncertainties using contemporary observations,

1. there must be a relationship between contemporary variability and future trends on longer time scales within the model, and

Reducing Uncertainties Using Observations

To reduce feedback uncertainties using contemporary observations,

1. there must be a relationship between contemporary variability and future trends on longer time scales within the model, and
2. it must be possible to constrain contemporary variability in the model using observations.

Reducing Uncertainties Using Observations

To reduce feedback uncertainties using contemporary observations,

1. there must be a relationship between contemporary variability and future trends on longer time scales within the model, and
2. it must be possible to constrain contemporary variability in the model using observations.

Example #1

Hall and Qu (2006) evaluated the strength of the springtime snow albedo feedback (SAF; $\Delta\alpha_s/\Delta T_s$) from 17 models used for the IPCC AR4 and compared them with the observed springtime SAF from ISCCP and ERA-40 reanalysis.

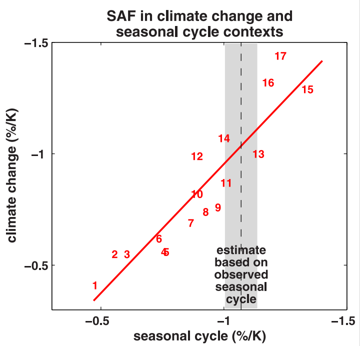

Reducing Uncertainties Using Observations

To reduce feedback uncertainties using contemporary observations,

1. there must be a relationship between contemporary variability and future trends on longer time scales within the model, and
2. it must be possible to constrain contemporary variability in the model using observations.

Example #2

Cox et al. (2013) used the observed relationship between the CO_2 growth rate and tropical temperature as a constraint to reduce uncertainty in the land carbon storage sensitivity to climate change (γ_L) in the tropics using C^4MIP models.

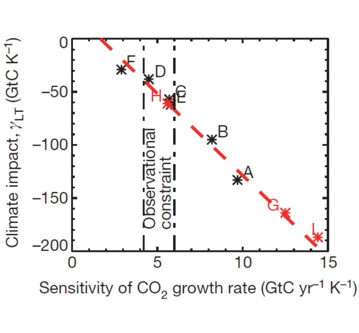

I developed a new emergent constraint from carbon inventories.

A relationship exists between contemporary and future atmospheric CO_2 levels over decadal time scales because carbon model biases persist over decadal time scales.

Observed contemporary atmospheric CO_2 mole fraction is represented by the vertical line at 384.6 $\pm$ 0.5 ppm.

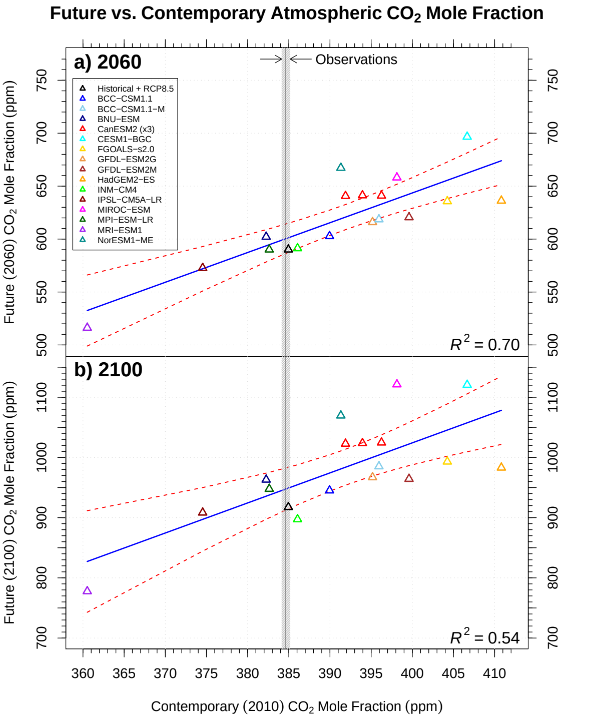

Removing pre-industrial CO_2 mole fraction biases from models, we found the relationship held, confirming the robustness of our result.

Observed contemporary anthropogenic atmospheric carbon inventory is represented by the vertical line at 213.4 ± 6.5 Pg C, which incorporates 1850 CO_2 mole fraction uncertainties.

Adding uncertainties from fossil fuel emissions increased the uncertainty to ± 12.7 Pg C.

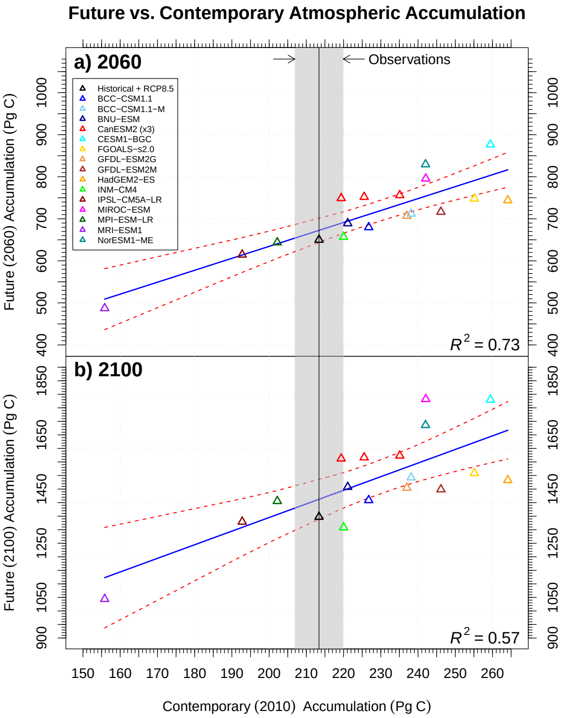

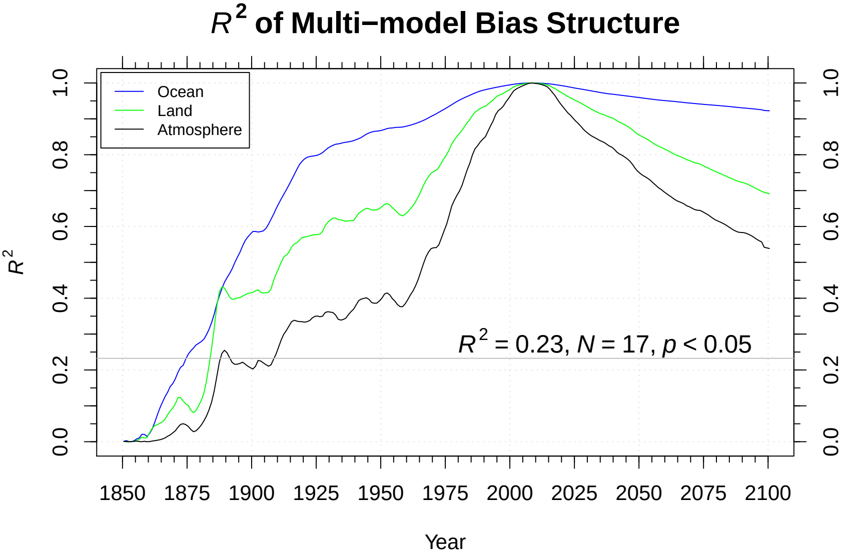

The coefficients of determination (R^2) for the multi-model bias structure relative to the set of CMIP5 model atmospheric CO_2 mole fractions (black), and oceanic (blue) and land (green) anthropogenic carbon inventories in 2010. Atmospheric CO_2 mole fractions are statistically significant for 1910–2100. Bias persistence was highest for the ocean, followed by land, and then by the atmosphere.

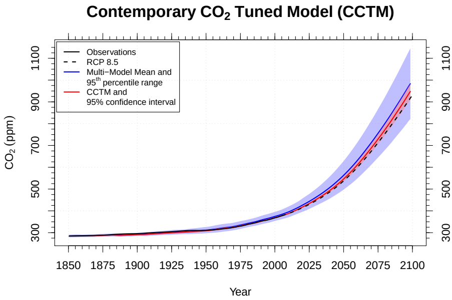

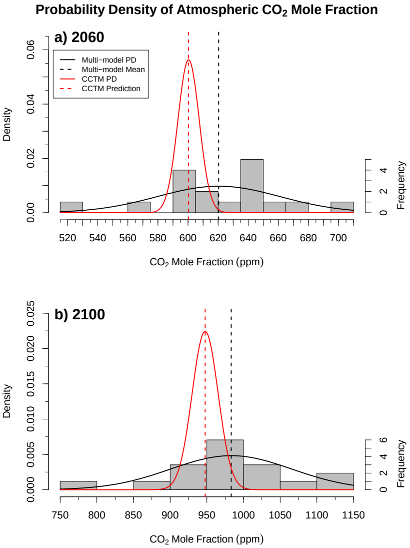

I used this regression to create a contemporary CO_2 tuned model (CCTM) estimate of the atmospheric CO_2 trajectory for the 21st century.

- Peak probability densities of CO_2 mole fraction predictions were lower for the CCTM than the multi-model means.
- The ranges of uncertainty were smaller by almost a factor of 6 at 2060 and almost a factor of 5 at 2100.

Best estimate using Mauna Loa CO_2

At 2060: 600 ± 14 ppm, 21 ppm below the multi-model mean
At 2100: 947 ± 35 ppm, 32 ppm below the multi-model mean

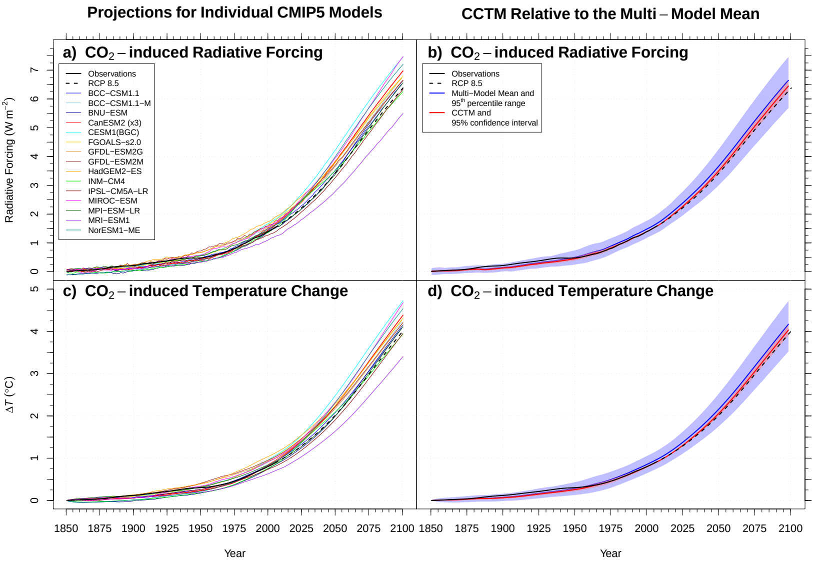

I calculated the CO_2 radiative forcing and used an impulse response function (tuned to the mean transient climate response of CMIP5 models) to equitably compute the resulting CO_2-induced temperature change (ΔT_{CO_2}) for models and the CCTM. The CO_2 biases for individual models contributed to ΔT_{CO_2} biases of -0.7°C to $+0.6^\circ$C by 2100, relative to the CCTM estimate.

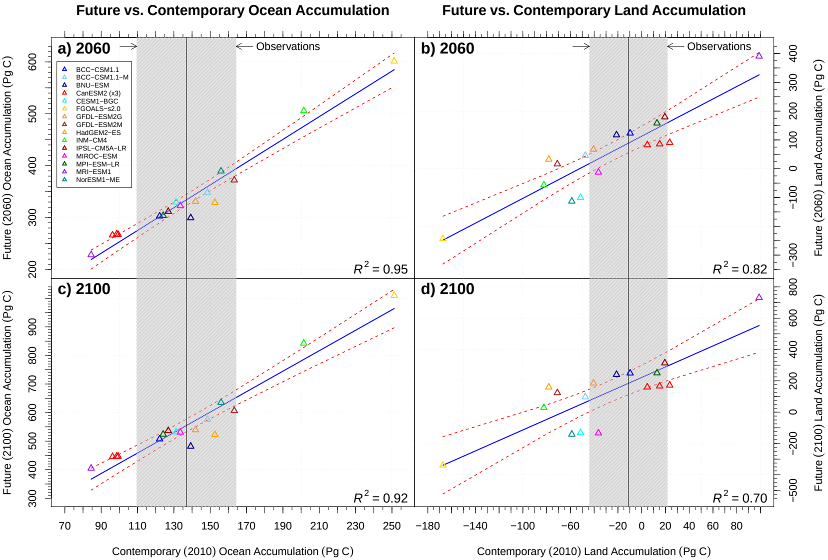

I also developed a multi-model constraint on the evolution of ocean and land anthropogenic inventories. Since observational uncertainties are higher for ocean and land, uncertainties in future estimates cannot be reduced as much as for atmospheric CO_2.

Question 2

Can we use contemporary CO_2 observations to constrain future CO_2 projections?

- Yes.
- I developed a new emergent constraint from anthropogenic carbon inventories in atmosphere, ocean, and land reservoirs.
- Land and ocean processes contributing to contemporary carbon cycle biases persist over decadal timescales.
- I used the relationship between contemporary and future atmospheric CO_2 levels to create a contemporary CO_2 tuned model (CCTM) estimate for the 21^{st} century.
  - At 2060: 600 ± 14 ppm, 21 ppm below the multi-model mean.
  - At 2100: 947 ± 35 ppm, 32 ppm below the multi-model mean.
- Uncertainties in future climate predictions may be reduced by improving models to match the long-term time series of CO_2 from Mauna Loa and other monitoring stations.

Implications of CO_2 Biases in ESMs

- Most of the model-to-model variability of CO_2 in the 21st century was traced to biases that existed at the end of the observational record.
- Future fossil fuel emissions targets designed to stabilize CO_2 levels would be too low if estimated from the multi-model mean of ESMs.
- Models could be improved through **extensive comparison with sustained observations** and **community model benchmarking**.


AGU PUBLICATIONS
JGR
Journal of Geophysical Research: Biogeosciences

RESEARCH ARTICLE
10.1002/2013JG002381

Key Points:
- We analyzed emission-driven simulations from 15 Earth System Models (ESMs)
- Most ESMs had a small positive bias in contemporary atmospheric CO_2 predictions
- We used a linear relationship to create a trajectory of future atmospheric CO_2

Supporting Information:
- Readme
- Supplementary Materials

Correspondence to:
F. M. Hoffman,
forrest@climatemodeling.org

Citation:
Hoffman, F. M., J. T. Randerson, V. K. Arora, Q. Bao, P. Cadule, D. Ji, C. D. Jones, M. Kawamiya, S. Khatiwala, K. Lindsay, A. Obata, E. Shevliakova, K. D. Six, J. F. Tjiputra, E. M. Volodin, and T. Wu (2014), Causes and implications of persistent atmospheric carbon dioxide biases in Earth System Models, *J. Geophys. Res. Biogeosci.*, *119*, 141–162, doi:10.1002/2013JG002381.

Received 13 MAY 2013
Accepted 17 DEC 2013
Accepted article online 19 DEC 2013
Published online 15 FEB 2014

Causes and implications of persistent atmospheric carbon dioxide biases in Earth System Models

F. M. Hoffman[1,2], J. T. Randerson[1], V. K. Arora[3], Q. Bao[4], P. Cadule[5], D. Ji[6], C. D. Jones[7], M. Kawamiya[8], S. Khatiwala[9], K. Lindsay[10], A. Obata[11], E. Shevliakova[12], K. D. Six[13], J. F. Tjiputra[14], E. M. Volodin[15], and T. Wu[16]

[1]Department of Earth System Science, University of California, Irvine, California, USA, [2]Climate Change Science Institute and Computational Earth Sciences Group, Oak Ridge National Laboratory, Oak Ridge, Tennessee, USA, [3]Canadian Center for Climate Modeling and Analysis, Meteorological Service of Canada, Victoria, British Columbia, Canada, [4]State Key Laboratory of Numerical Modeling for Atmospheric Sciences and Geophysical Fluid Dynamics, Institute of Atmospheric Physics, Chinese Academy of Sciences, Beijing, China, [5]Institut Pierre Simon Laplace, Laboratoire des Sciences du Climat et de l'Environnement, Gif sur Yvette CEDEX, France, [6]State Key Laboratory of Earth Surface Processes and Resource Ecology, College of Global Change and Earth System Science, Beijing Normal University, Beijing, China, [7]Hadley Center, U.K. Met Office, Exeter, UK, [8]Research Institute for Global Change, Japan Agency for Marine-Earth Science and Technology, Kanagawa, Japan, [9]Lamont Doherty Earth Observatory, Columbia University, Palisades, New York, USA, [10]Climate and Global Dynamics Division, National Center for Atmospheric Research, Boulder, Colorado, USA, [11]Meteorological Research Institute, Japan Meteorological Agency, Ibaraki, Japan, [12]Geophysical Fluid Dynamics Laboratory, Princeton University, Princeton, New Jersey, USA, [13]Max Planck Institute for Meteorology, Hamburg, Germany, [14]Uni Climate, Uni Research, Bergen, Norway, [15]Institute of Numerical Mathematics, Russian Academy of Science, Moscow, Russia, [16]Climate System Modeling Division, Beijing Climate Center, China Meteorological Administration, Beijing, China

Abstract The strength of feedbacks between a changing climate and future CO_2 concentrations is uncertain and difficult to predict using Earth System Models (ESMs). We analyzed emission-driven simulations—in which atmospheric CO_2 levels were computed prognostically—for historical (1850–2005) and future periods (Representative Concentration Pathway (RCP) 8.5 for 2006–2100) produced by 15 ESMs for the Fifth Phase of the Coupled Model Intercomparison Project (CMIP5). Comparison of ESM prognostic atmospheric CO_2 over the historical period with observations indicated that ESMs, on average, had a small positive bias in predictions of contemporary atmospheric CO_2. Weak ocean carbon uptake in many ESMs contributed to this bias, based on comparisons with observations of ocean and atmospheric anthropogenic carbon inventories. We found a significant linear relationship between contemporary atmospheric CO_2 biases and future CO_2 levels for the multimodel ensemble. We used this relationship to create a contemporary CO_2 tuned model (CCTM) estimate of the atmospheric CO_2 trajectory for the 21st century. The CCTM yielded CO_2 estimates of 600 ± 14 ppm at 2060 and 947 ± 35 ppm at 2100, which were 21 ppm and 32 ppm below the multimodel mean during these two time periods. Using this emergent constraint approach, the likely ranges of future atmospheric CO_2, CO_2-induced radiative forcing, and CO_2-induced temperature increases for the RCP 8.5 scenario were considerably narrowed compared to estimates from the full ESM ensemble. Our analysis provided evidence that much of the model-to-model variation in projected CO_2 during the 21st century was tied to biases that existed during the observational era and that model differences in the representation of concentration-carbon feedbacks and other slowly changing carbon cycle processes appear to be the primary driver of this variability. By improving models to more closely match the long-term time series of CO_2 from Mauna Loa, our analysis suggests that uncertainties in future climate projections can be reduced.

1. Introduction

Anthropogenic emissions of radiatively active greenhouse gases into the atmosphere, especially carbon dioxide (CO_2), are rapidly increasing the burden of these gases and altering the Earth's climate [*IPCC*, 2007; *Raupach and J. G. Canadell*, 2010]. This perturbation of the global carbon cycle is expected to induce feedbacks from the terrestrial biosphere and oceans on future CO_2 concentrations and the climate system. These climate–carbon cycle feedbacks are highly uncertain, difficult to predict, and potentially large [*Denman et al.*, 2007]. Understanding and predicting the strength and direction of feedbacks is critically important

Hoffman, Forrest M., James T. Randerson, Vivek K. Arora, Qing Bao, Patricia Cadule, Duoying Ji, Chris D. Jones, Michio Kawamiya, Samar Khatiwala, Keith Lindsay, Atsushi Obata, Elena Shevliakova, Katharina D. Six, Jerry F. Tjiputra, Evgeny M. Volodin, and Tongwen Wu (2014), Causes and Implications of Persistent Atmospheric Carbon Dioxide Biases in Earth System Models, *J. Geophys. Res. Biogeosci.*, 119(2):141162, doi:10.1002/2013JG002381.

Model, Experiment, and Data Integration Strategy

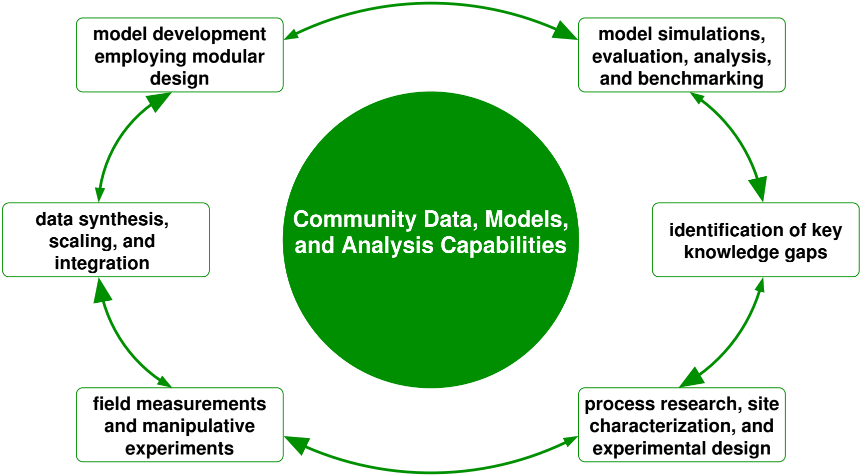

Model, Experiment, and Data Integration Strategy

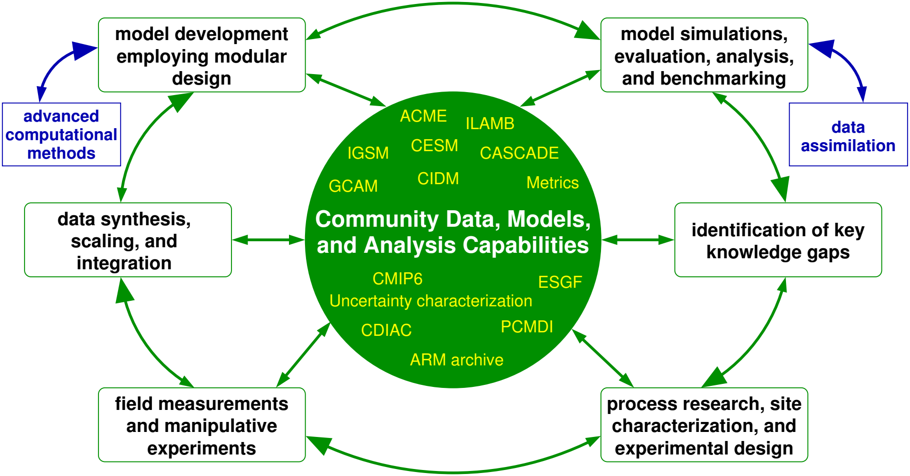

Model, Experiment, and Data Integration Strategy

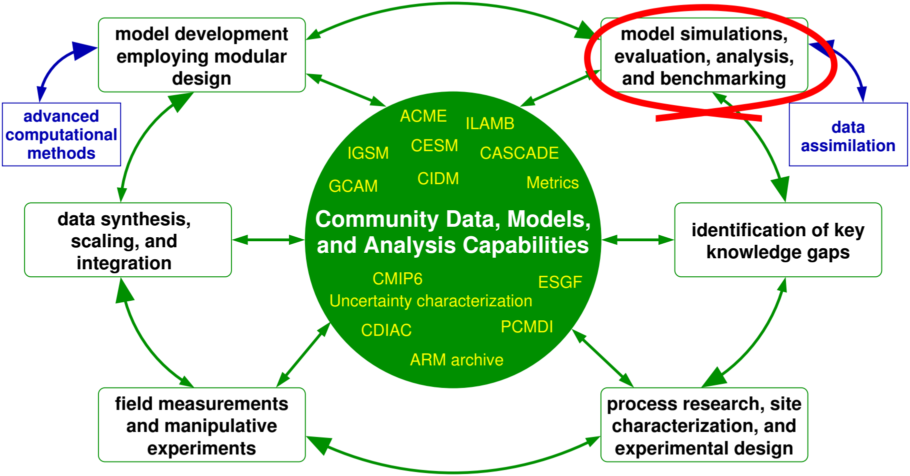

Biogeochemistry–Climate Feedbacks SFA Diagram

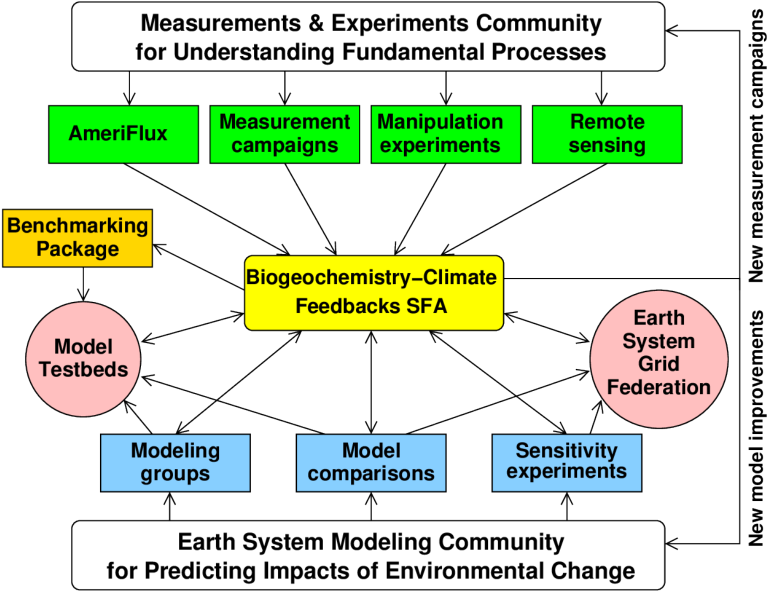

What is ILAMB?

- The **International Land Model Benchmarking (ILAMB)** project seeks to develop internationally accepted standards for land model evaluation.
- Model **benchmarking** can diagnose impacts of model development and guide synthesis efforts like IPCC.
- **Effective benchmarks** must draw upon a broad set of independent observations to evaluate model performance on multiple temporal and spatial scales.
- A free, **open source analysis and diagnostics software package** for community use will enhance model intercomparison projects.

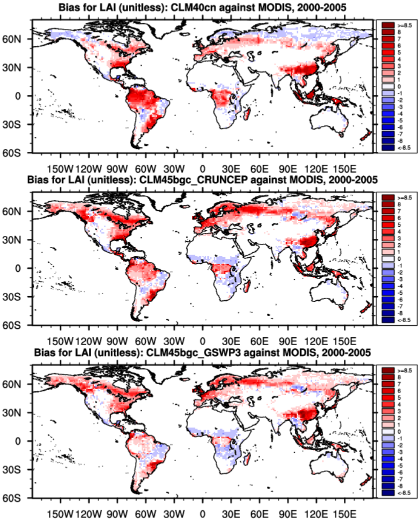

Bias in mean annual leaf area index from comparison of three versions CLM with MODIS.

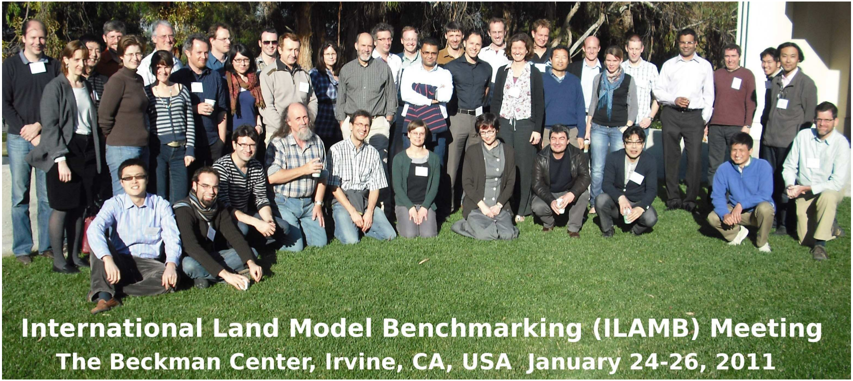

- We co-organized inaugural meeting and ∼45 researchers participated from the United States, Canada, the United Kingdom, the Netherlands, France, Germany, Switzerland, China, Japan, and Australia.
- **ILAMB Goals:** Develop internationally accepted benchmarks for model performance, advocate for design of open-source software system, and strengthen linkages between experimental, monitoring, remote sensing, and climate modeling communities.
- Methodology for model–data comparison and baseline standard for performance of land model process representations (Luo et al., 2012).

Benchmarking Metholdology (Luo et al., 2012)

- Based on this methodology and prior work in C-LAMP, we developed a new model benchmarking package for ILAMB.
- Prototype is ready for use in NCL and a new version is under development using python.

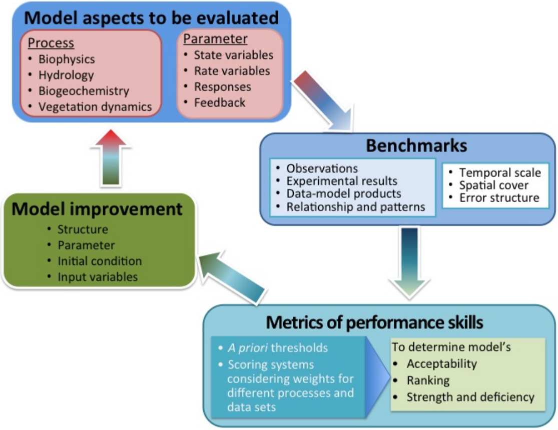

(Luo et al., 2012)

ILAMB Prototype developed by Mingquan Mu at UCI

- Assesses 24 variables in 4 categories frm ∼45 datasets
  - aboveground live biomass, burned area, carbon dioxide, gross primary production, leaf area index, global net ecosystem carbon balance, net ecosystem exchange, ecosystem respiration, soil carbon
  - evapotranspiration, latent heat, terrestrial water storage anomaly
  - albedo, surface upward SW radiation, surface net SW radiation, surface upward LW radiation, surface net LW radiation, surface net radiation, sensible heat
  - surface air temperature, precipitation, surface relative humidity, surface downward SW radiation, surface downward LW radiation
- Graphics and scoring system
  - annual mean, bias, RMSE, seasonal cycle, spatial distribution, interannual coefficient of variation, spatial distribution, long-term trend
- Software is available at
  `http://redwood.ess.uci.edu/mingquan/www/ILAMB/index.html`

ILAMB Prototype: Global Variables for 12 Models

Global Variables (Info for Weightings)

	MeanModel	bcc-csm1-1-m	BNU-ESM	CanESM2	CESM1-BGC	GFDL-ESM2G	HadGEM2-ES	inmcm4	IPSL-CM5A-LR	MIROC-ESM	MPI-ESM-LR	MRI-ESM1	NorESM1-ME
Aboveground Live Biomass	0.68	0.52	0.50	0.61	0.65	0.58	0.67	0.54	0.68	0.52	0.51	0.67	0.65
Burned Area	0.38	-	-	-	0.37	-	-	-	-	-	0.38	-	0.38
Carbon Dioxide	0.85	-	0.65	0.65	0.78	0.65	-	-	-	0.79	0.68	0.68	0.75
Gross Primary Productivity	0.77	0.72	0.73	0.64	0.70	0.67	0.68	0.70	0.67	0.69	0.69	0.53	0.70
Leaf Area Index	0.66	0.66	0.41	0.60	0.53	0.49	0.59	0.68	0.66	0.62	0.68	0.43	0.50
Global Net Ecosystem Carbon Balance	0.58	-	0.38	0.27	0.38	0.18	-	0.46	0.25	0.38	0.42	0.27	0.40
Net Ecosystem Exchange	0.49	0.47	0.47	0.39	0.48	0.49	0.46	0.44	0.53	0.48	0.50	0.48	0.48
Ecosystem Respiration	0.75	0.72	0.72	0.65	0.67	0.71	0.66	0.70	0.67	0.68	0.68	0.47	0.66
Soil Carbon	0.55	0.50	0.42	0.56	0.38	0.51	0.51	0.53	0.57	0.53	0.41	0.53	0.39
Summary	0.64	0.59	0.54	0.54	0.55	0.53	0.59	0.57	0.57	0.58	0.54	0.51	0.55
Evapotranspiration	0.75	0.73	0.72	0.72	0.73	0.70	0.74	0.69	0.75	0.70	0.73	0.73	0.72
Latent Heat	0.80	0.76	0.77	0.77	0.78	0.74	0.77	0.72	0.77	0.75	0.76	0.78	0.76
Terrestrial Water Storage Anomaly	0.53	0.45	0.35	0.54	0.48	0.43	-	0.52	0.45	0.52	0.55	0.47	0.45
Summary	0.69	0.65	0.61	0.68	0.66	0.62	0.75	0.64	0.65	0.66	0.68	0.66	0.64
Albedo	0.72	0.71	0.61	0.71	0.73	0.69	0.74	0.67	0.71	0.67	0.73	0.64	0.72
Surface Upward SW Radiation	0.78	0.73	0.67	0.74	0.78	0.74	0.77	0.74	0.74	0.72	0.78	0.67	0.76
Surface Net SW Radiation	0.84	0.86	0.84	0.85	0.85	0.86	0.85	0.84	0.82	0.83	0.87	0.85	0.85
Surface Upward LW Radiation	0.90	0.91	0.91	0.91	0.92	0.91	0.92	0.89	0.90	0.91	0.92	0.92	0.92
Surface Net LW Radiation	0.81	0.82	0.81	0.79	0.82	0.81	0.83	0.79	0.78	0.78	0.81	0.82	0.81
Surface Net Radiation	0.78	0.79	0.76	0.80	0.80	0.80	0.79	0.74	0.77	0.76	0.80	0.78	0.80
Sensible Heat	0.76	0.69	0.70	0.71	0.75	0.69	0.75	0.66	0.69	0.69	0.69	0.72	0.72
Summary	0.79	0.78	0.75	0.78	0.80	0.78	0.80	0.75	0.76	0.76	0.79	0.77	0.79
Surface Air Temperature	0.87	0.87	0.85	0.85	0.88	0.85	0.87	0.85	0.87	0.85	0.88	0.88	0.87
Precipitation	0.70	0.67	0.66	0.67	0.70	0.68	0.72	0.68	0.68	0.68	0.70	0.69	0.69
Surface Relative Humidity	0.81	-	0.80	0.76	0.82	-	-	0.79	0.82	-	-	0.83	0.81
Surface Downward SW Radiation	0.86	0.88	0.87	0.87	0.88	0.87	0.87	0.87	0.83	0.86	0.88	0.86	0.88
Surface Downward LW Radiation	0.90	0.92	0.91	0.91	0.92	0.92	0.92	0.90	0.89	0.91	0.93	0.91	0.91
Summary	0.82	0.82	0.81	0.80	0.83	0.82	0.84	0.81	0.81	0.81	0.84	0.83	0.82
Overall	0.69	0.51	0.59	0.60	0.64	0.56	0.49	0.57	0.57	0.59	0.61	0.59	0.63

ILAMB Prototype: Global Variables for 12 Models

Global Variables (Info for Weightings)

	MeanModel	bcc-csm1-1-m	BNU-ESM	CanESM2	CESM1-BGC	GFDL-ESM2G	HadGE
Aboveground Live Biomass	0.68	0.52	0.50	0.61	0.65	0.58	0.6
Burned Area	0.38	-	-	-	0.37	-	-
Carbon Dioxide	0.85	-	0.65	0.65	0.78	0.65	-
Gross Primary Productivity	0.77	0.72	0.73	0.64	0.70	0.67	0.6
Leaf Area Index	0.66	0.66	0.41	0.60	0.53	0.49	0.5
Global Net Ecosystem Carbon Balance	0.58	-	0.38	0.27	0.38	0.18	-
Net Ecosystem Exchange	0.49	0.47	0.47	0.39	0.48	0.49	0.4
Ecosystem Respiration	0.75	0.72	0.72	0.65	0.67	0.71	0.6
Soil Carbon	0.55	0.50	0.42	0.56	0.38	0.51	0.5
Summary	0.64	0.59	0.54	0.54	0.55	0.53	0.5
Evapotranspiration	0.75	0.73	0.72	0.72	0.73	0.70	0.7
Latent Heat	0.80	0.76	0.77	0.77	0.78	0.74	0.7
Terrestrial Water Storage Anomaly	0.53	0.45	0.35	0.54	0.48	0.43	-
Summary	0.69	0.65	0.61	0.68	0.66	0.62	0.7
Albedo	0.72	0.71	0.61	0.71	0.73	0.69	0.7
Surface Upward SW Radiation	0.78	0.73	0.67	0.74	0.78	0.74	0.7
Surface Net SW	0.84	0.86	0.84	0.85	0.85	0.86	0.8

Scoring for Global GPP from Fluxnet-MTE

Diagnostic Summary for Gross Primary Productivity: Model vs. FLUXNET-MTE

	Global Patterns				Regional and Seasonal Patterns	Scoring (Info)				
	Annual Mean (PgC/yr)	Bias (PgC/yr)	RMSE (PgC/mon)	Phase Difference (months)	Regional Means	Global Bias	RMSE	Seasonal Cycle	Spatial Distribution	Overall
Benchmark [Jung et al. (2009)]	118.4	-	-	0.0	access to plots	-	-	-	-	-
MeanModel	145.3	26.9	4.7	0.6	access to plots	0.77	0.73	0.78	0.94	0.79
bcc-csm1-1-m	114.4	-4.0	6.0	-0.2	access to plots	0.72	0.64	0.80	0.89	0.74
BNU-ESM	102.0	-16.4	6.2	0.1	access to plots	0.69	0.66	0.78	0.84	0.73
CanESM2	129.2	10.8	7.3	0.8	access to plots	0.64	0.60	0.68	0.70	0.64
CESM1-BGC	130.3	11.9	5.8	0.5	access to plots	0.69	0.65	0.76	0.87	0.72
GFDL-ESM2G	175.1	56.7	9.8	0.5	access to plots	0.66	0.54	0.73	0.83	0.66
HadGEM2-ES	145.9	27.5	7.4	0.3	access to plots	0.65	0.58	0.78	0.79	0.68
inmcm4	111.4	-7.0	5.6	0.3	access to plots	0.71	0.66	0.78	0.83	0.73
IPSL-CM5A-LR	166.6	48.2	8.8	0.4	access to plots	0.63	0.56	0.77	0.84	0.67
MIROC-ESM	131.7	13.3	6.2	0.2	access to plots	0.72	0.66	0.74	0.86	0.73
MPI-ESM-LR	169.9	51.5	7.4	0.3	access to plots	0.67	0.62	0.70	0.89	0.70
MRI-ESM1	236.1	117.7	12.5	0.2	access to plots	0.45	0.43	0.79	0.59	0.54
NorESM1-ME	130.4	12.0	6.5	0.5	access to plots	0.66	0.62	0.76	0.84	0.70

Notes: In calculating overall score, rmse score contributes double in comparison with all other scores.

Annual Mean Global GPP

Models vs. FLUXNET-MTE

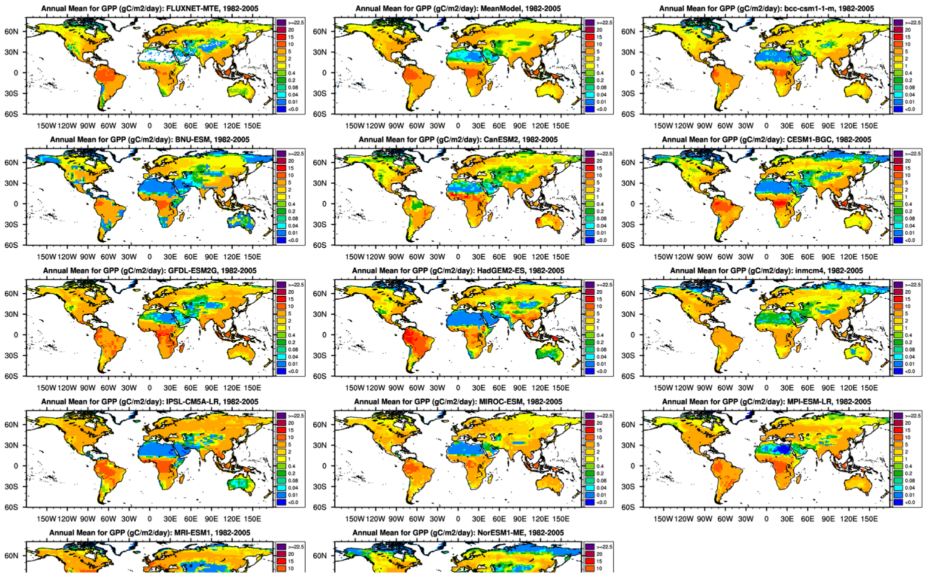

Seasonal Cycle of Regional GPP

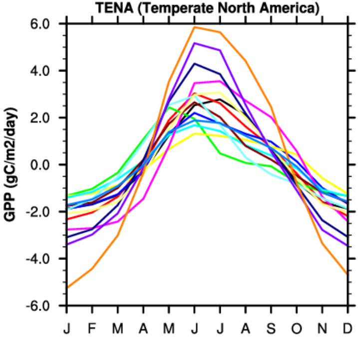

Model	Annual	Bias	RMSE
FLUXNET-MTE	2.36	-999.00	-999.00
MeanModel	2.99	0.63	0.74
bcc-csm1-1-m	1.82	-0.54	1.31
BNU-ESM	2.17	-0.19	0.62
CanESM2	1.76	-0.60	1.08
CESM1-BGC	2.45	0.08	0.78
GFDL-ESM2G	2.85	0.49	1.16
HadGEM2-ES	2.12	-0.24	0.72
inmcm4	3.06	0.70	1.20
IPSL-CM5A-LR	3.95	1.59	1.90
MIROC-ESM	2.48	0.12	0.35
MPI-ESM-LR	4.27	1.91	2.38
MRI-ESM1	6.13	3.76	4.46
NorESM1-ME	2.84	0.48	0.74

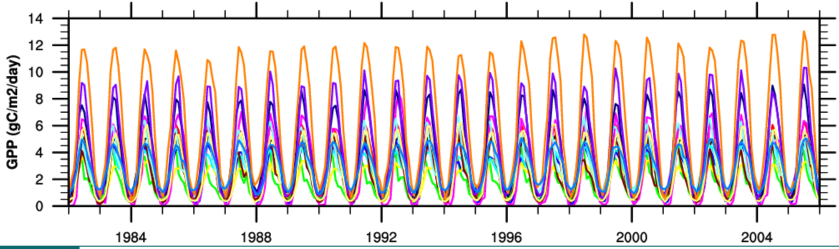

Seasonal Cycle of Site GPP

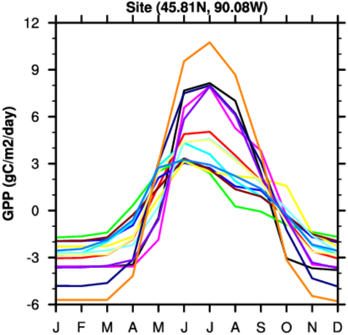

Model	Annual	Bias	RMSE
FLUXNET	3.62	-999.00	-999.00
MeanModel	3.11	-0.51	2.49
bcc-csm1-1-m	1.79	-1.83	4.42
BNU-ESM	2.00	-1.62	3.81
CanESM2	2.32	-1.30	3.69
CESM1-BGC	3.04	-0.58	3.19
GFDL-ESM2G	3.59	-0.03	2.87
HadGEM2-ES	2.06	-1.56	3.77
inmcm4	2.79	-0.83	2.75
IPSL-CM5A-LR	4.85	1.23	2.37
MIROC-ESM	2.81	-0.81	2.85
MPI-ESM-LR	3.68	0.06	1.72
MRI-ESM1	5.76	2.14	3.45
NorESM1-ME	2.69	-0.93	3.45

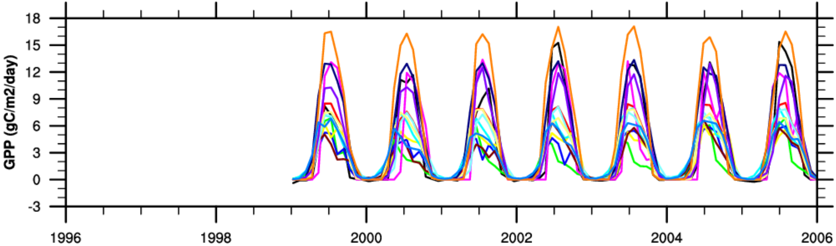

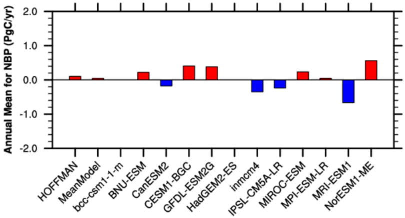

Global Net Ecosystem Carbon Balance

Long term carbon storage

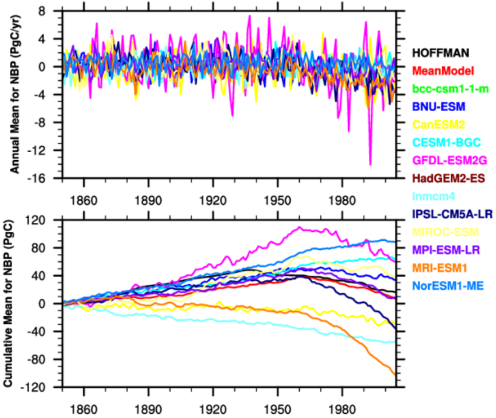

Functional Relationships: GPP vs. Precipitation

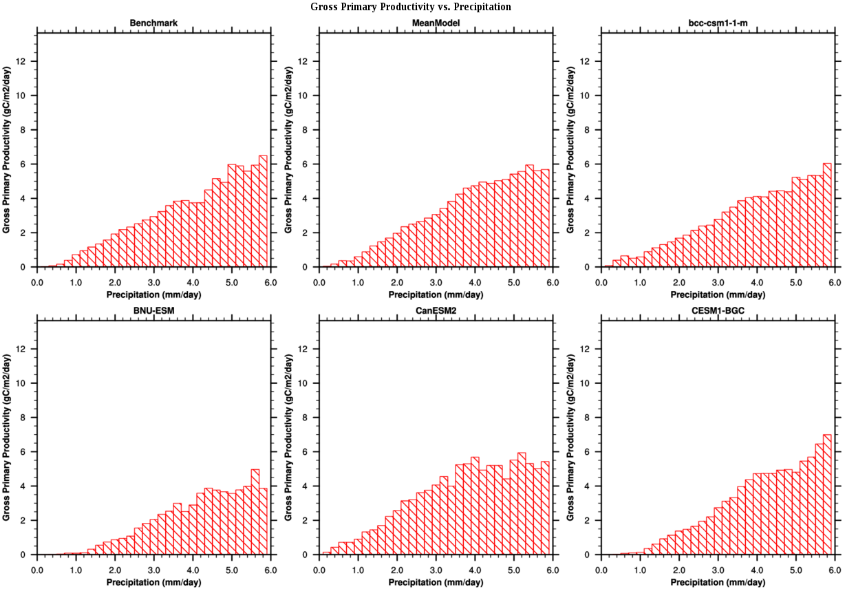

ILAMB Metrics Document

B. Root Mean Square Error Metric

For different variables, we use 2 different methods to calculate their global mean RMSE scores. For above ground biomass (biomass), burned area (burntarea), evapotranspiration (et), gross primary production (gpp), lead area index (lai), latent heat (le), net ecosystem exchange (nee), precipitation (pr), ecosystem respiration (reco), sensible heat (sh) and soil carbon (soilc), we use mass weighting (B3.1). For other variables, we use area weighting (B3.2).

$$M_i = 1 - \frac{RMSE_i}{\Phi_{obs,i}} \qquad \text{(B1)}$$

$$M_i' = e^{M_i} / e \qquad \text{(B2)}$$

Mass weighting to calculate global mean RMSE score:

$$M = \frac{\sum_{i=1}^{ncells} M_i' \times A_i \times |AM_{obs,i}|}{\sum_{i=1}^{ncells} A_i \times |AM_{obs,i}|} \qquad \text{(B3.1)}$$

Area weighting to calculate global mean RMSE score:

$$M = \frac{\sum_{i=1}^{ncells} M_i' \times A_i}{\sum_{i=1}^{ncells} A_i} \qquad \text{(B3.2)}$$

We use Eqs. B1-2 and Eq. B3.1 or B3.2 to calculate root mean square error metric score M_i at grid cell or site i and its global mean M, respectively. Where $\Phi_{obs,i}$ is the root mean square for monthly mean annual cycle of the observation at grid cell i (for grid data) or site i (for site observation), and $RMSE_i$ is the root mean square error between model and observation. $AM_{obs,i}$ is annual mean of the observation at grid cell or site i. $|AM_{obs,i}|$ is to calculate its absolute value. A_i is the area for grid cell or site i. *ncells* is the number if all land grid cells or sites where observation data is available. If the observation is site data, we set A_i equal to 1 (*Ref: David Lawrence's personal Communication*). This metric is used to compare magnitude and phase difference of the monthly mean annual cycle between the model and the observation.

C. Spatial Distribution Metric

$$M = \frac{4(1+R)}{(\sigma_f + 1/\sigma_f)^2 (1+R_0)} \qquad \text{(C)}$$

We use Eq. C to calculate spatial distribution metric score M. R is the spatial correlation coefficient of the annual mean between model and observation. R_o is their ideal maximum correlation. Here, we set R_o equal to 1 for all models. σ_f is ratio for standard deviation of model to that of observation (*Ref: Taylor, J. Geophys. Res., 106, 2001*). This metric is used to compare magnitude and spatial pattern of annual mean of model with observation.

D. Seasonal Cycle Phase Metric

For different variables, we use 2 different methods to calculate their global mean phase scores. For above ground biomass (biomass), burned area (burntarea), evapotranspiration (et), gross primary production (gpp), lead area index (lai), latent heat (le), net ecosystem exchange (nee), precipitation (pr), ecosystem respiration (reco), sensible heat (sh) and soil carbon (soilc), we use mass weighting (D2.1). For other variables, we use area weighting (D2.2).

$$M_i = (1 + \cos\vartheta_i) / 2 \qquad \text{(D1)}$$

Mass weighting to calculate global mean phase score:

$$M = \frac{\sum_{i=1}^{ncells} M_i \times A_i \times |AM_{obs,i}|}{\sum_{i=1}^{ncells} A_i \times |AM_{obs,i}|} \qquad \text{(D2.1)}$$

Area weighting to calculate global mean phase score:

$$M = \frac{\sum_{i=1}^{ncells} M_i \times A_i}{\sum_{i=1}^{ncells} A_i} \qquad \text{(D2.2)}$$

We use Eqs. D1 and D2.1 or D2.2 to calculate seasonal cycle phase metric score M_i at grid cell or site i and its global mean M, respectively. ϑ_i is the difference of the angle between the month of the maximum value for the model and that for the observation at grid cell i (for the grid data) or site i (for the site data). $AM_{obs,i}$ is annual mean of the observation at grid cell or site i. $|AM_{obs,i}|$ is to calculate its absolute value. A_i is the area for grid cell or site i. *ncells* is the number of all land grid cells or sites where observation data is available. If the observation is site data, we set A_i equal to 1 (*Ref: Prentice, et al., GBC, 25, 2011*). This metric is used to compare phase difference of the monthly mean annual cycle between the model and the observation.

E. Interannual Variability Metric

ILAMB Scoring Rules

Rules for scoring system

Score	Certainty of data	Scale appropriateness and coverage	Overall importance of constraint or process
1	Uncertainty estimates not available; significant methodological issues may influence data quality	Site level observations with limited regional coverage and/or short temporal duration	Observations that have limited influence on carbon cycle processes; includes some driver datasets and land surface measurements (e.g., Lin)
2	Uncertainty estimates not available; some methodological issues may influence data quality	Partial regional coverage; data sets providing up to 1 year of coverage	Driver observations or land surface measurements that have direct influence on carbon cycle processes (e.g., PPT, Tair, and Sin)
3	Uncertainty estimates not available; some peer-review evaluation of quality; minor methodological issues may remain	Regional coverage for at least 1 year; mismatches may exist between site-level and model grid cells	Biosphere process that contributes to carbon dynamics; data are a useful constraint for thi specific process
4	Qualitative uncertainty information available from peer-review evaluations; methodology is well accepted	Important regional coverage; at least 1 year or more of observations	Important biosphere process regulating carbon cycle dynamics; data are moderately well-suited for constraining this process
5	Well defined and traceable uncertainty estimates; relatively low uncertainty estimates relative to range of model estimates; uncertainties less than ± 20% at regional scales	Global scale in coverage; time series spanning multiple years; data products appropriate in scale for comparing directly with model grid cells	Critical process or constraint regulating climate-carbon or carbon-concentration feedbacks; data are well suited for discriminating among different model estimates

ILAMB Model Scoring by Variable

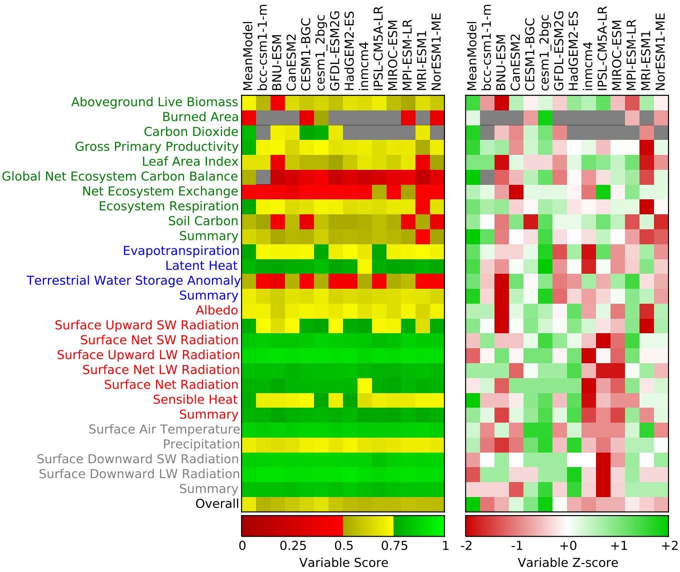

ILAMB Next Generation Layout

ILAMB Benchmark Results

Overview | **Results Table** | Model Comparisons

Columns...

	CLM40cn	CLM45bgc_CRUNCEP	CLM45bgc_GSWP3
Biomass	0.40	0.40	0.41
Burned Area	0.62	0.66	0.65
Gross Primary Productivity	0.70	0.72	0.73
Fluxnet (36.0%)	0.69	0.72	0.73
Fluxnet-MTE (60.0%)	0.71	0.72	0.73
Leaf Area Index	0.62	0.60	0.63
Global Net Ecosystem Carbon Balance	0.17	0.23	0.20
Net Ecosystem Exchange	0.55	0.55	0.55
Ecosystem Respiration	0.67	0.70	0.72
Soil Carbon	0.55	0.58	0.65
Evapotranspiration	0.73	0.75	0.75
Latent Heat	0.73	0.75	0.75
Terrestrial Water Storage Anomaly	0.30	0.31	0.31
Albedo	0.72	0.72	0.72
Surface Upward SW Radiation	0.77	0.77	0.78
Surface Net SW Radiation	0.80	0.80	0.81
Surface Upward LW Radiation	0.81	0.81	0.82
Surface Net LW Radiation	0.73	0.73	0.77
Surface Net Radiation	0.77	0.77	0.78
Sensible Heat	0.72	0.72	0.74
Surface Air Temperature	0.83	0.83	0.84
Precipitation	0.76	0.76	0.78

ILAMB Next Generation Layout

www.climatemodeling.org/~nate/ILAMB/EcosystemandCarbonCycle/GrossPrimaryProductivity/Fluxnet-MTE//Fluxnet-MTE.html

GrossPrimaryProductivity / Fluxnet-MTE / global / CLM40cn

Single Model | **All Models**

global

Model	Data	Period Mean [Pg yr-1]	Bias [Pg yr-1]	RMSE [Pg yr-1]	Phase Shift [d]	Bias Score [1]	RMSE Score [1]	Phase Score [1]	Interannual Variability Score [1]	Spatial Distribution Score [-]
Benchmark	[-]	115.711								
CLM40cn	[-]	130.054	17.551	77.741	-1.497	0.761	0.576	0.828	0.728	0.77
CLM45bgc_CRUNCEP	[-]	117.757	5.466	70.723	-2.595	0.784	0.557	0.832	0.711	0.899
CLM45bgc_GSWP3	[-]	107.227	-5.213	66.767	-1.556	0.794	0.556	0.82	0.731	0.922

Temporally integrated period mean

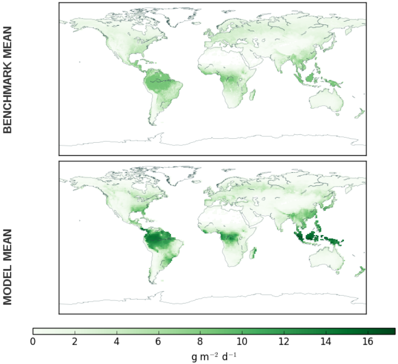

Future ILAMB Development and Application

- Current ILAMB Prototype was applied to:
  - Model development of the Community Land Model (CLM)
  - CMIP5 Historical and esmHistorical simulations
  - ACME Land Model evaluation
- Within U.S. Department of Energy projects:
  - NGEE Arctic, NGEE Tropics, and SPRUCE are adopting the framework for evaluating process parameterizations & integrating field observations
  - ACME is developing metrics for evaluation of new land model features
  - BGC Feedbacks is developing the framework and benchmarking MIPs
- Future (and past) projects where we hope to apply ILAMB:
  - CMIP6, including C^4MIP, LS3MIP, and LUMIP
  - TRENDY, MsTMIP, PLUME-MIP
  - NASA Permafrost Benchmark System (PBS) (Schaefer et al.)
- We will host the second ILAMB Workshop in the U.S. in Washington, DC, on May 16–18, 2016.

Acknowledgments

U.S. DEPARTMENT OF ENERGY
Office of Science

FOREST SERVICE
U S
DEPARTMENT OF AGRICULTURE

NSF

This research was sponsored by the Climate and Environmental Sciences Division (CESD) of the Biological and Environmental Research (BER) Program in the U. S. Department of Energy Office of Science and the National Science Foundation (AGS-1048890). This research used resources of the Oak Ridge Leadership Computing Facility (OLCF) at Oak Ridge National Laboratory (ORNL), which is managed by UT-Battelle, LLC, for the U. S. Department of Energy under Contract No. DE-AC05-00OR22725.

I wish to acknowledge the World Climate Research Programme's Working Group on Coupled Modelling, which is responsible for CMIP, and thank the climate modeling groups for producing and making available their model output. For CMIP the U. S. Department of Energy's Program for Climate Model Diagnosis and Intercomparison provides coordinating support and led development of software infrastructure in partnership with the Global Organization for Earth System Science Portals.

References

R. J. Andres, J. S. Gregg, L. Losey, G. Marland, and T. A. Boden. Monthly, global emissions of carbon dioxide from fossil fuel consumption. *Tellus B*, 63(3):309–327, July 2011. doi:10.1111/j.1600-0889.2011.00530.x.

R. J. Andres, T. A. Boden, F.-M. Bréon, P. Ciais, S. Davis, D. Erickson, J. S. Gregg, A. Jacobson, G. Marland, J. Miller, T. Oda, J. G. J. Olivier, M. R. Raupach, P. Rayner, and K. Treanton. A synthesis of carbon dioxide emissions from fossil-fuel combustion. *Biogeosci.*, 9(5):1845–1871, May 2012. doi:10.5194/bg-9-1845-2012.

P. M. Cox, D. Pearson, B. B. Booth, P. Friedlingstein, C. Huntingford, C. D. Jones, and C. M. Luke. Sensitivity of tropical carbon to climate change constrained by carbon dioxide variability. *Nature*, 494(7437):341–344, Feb. 2013. doi:10.1038/nature11882.

A. Hall and X. Qu. Using the current seasonal cycle to constrain snow albedo feedback in future climate change. *Geophys. Res. Lett.*, 33(3):L03502, Feb. 2006. doi:10.1029/2005GL025127.

W. W. Hargrove, J. P. Spruce, G. E. Gasser, and F. M. Hoffman. Toward a national early warning system for forest disturbances using remotely sensed phenology. *Photogramm. Eng. Rem. Sens.*, 75(10):1150–1156, Oct. 2009.

F. M. Hoffman. Analysis of reflected spectral signatures and detection of geophysical disturbance using hyperspectral imagery. Master's thesis, University of Tennessee, Department of Physics and Astronomy, Knoxville, Tennessee, USA, Nov. 2004.

F. M. Hoffman, J. T. Randerson, V. K. Arora, Q. Bao, P. Cadule, D. Ji, C. D. Jones, M. Kawamiya, S. Khatiwala, K. Lindsay, A. Obata, E. Shevliakova, K. D. Six, J. F. Tjiputra, E. M. Volodin, and T. Wu. Causes and implications of persistent atmospheric carbon dioxide biases in Earth System Models. *J. Geophys. Res. Biogeosci.*, 119(2):141–162, Feb. 2014. doi:10.1002/2013JG002381.

S. Khatiwala, T. Tanhua, S. Mikaloff Fletcher, M. Gerber, S. C. Doney, H. D. Graven, N. Gruber, G. A. McKinley, A. Murata, A. F. Ríos, and C. L. Sabine. Global ocean storage of anthropogenic carbon. *Biogeosci.*, 10(4):2169–2191, Apr. 2013. doi:10.5194/bg-10-2169-2013.

Y. Q. Luo, J. T. Randerson, G. Abramowitz, C. Bacour, E. Blyth, N. Carvalhais, P. Ciais, D. Dalmonech, J. B. Fisher, R. Fisher, P. Friedlingstein, K. Hibbard, F. Hoffman, D. Huntzinger, C. D. Jones, C. Koven, D. Lawrence, D. J. Li, M. Mahecha, S. L. Niu, R. Norby, S. L. Piao, X. Qi, P. Peylin, I. C. Prentice, W. Riley, M. Reichstein, C. Schwalm, Y. P. Wang, J. Y. Xia, S. Zaehle, and X. H. Zhou. A framework for benchmarking land models. *Biogeosci.*, 9(10):3857–3874, Oct. 2012. doi:10.5194/bg-9-3857-2012.

M. Meinshausen, S. Smith, K. Calvin, J. Daniel, M. Kainuma, J.-F. Lamarque, K. Matsumoto, S. Montzka, S. Raper, K. Riahi, A. Thomson, G. Velders, and D. P. van Vuuren. The RCP greenhouse gas concentrations and their extensions from 1765 to 2300. *Clim. Change*, 109(1):213–241, Nov. 2011. doi:10.1007/s10584-011-0156-z.

C. L. Sabine, R. A. Feely, N. Gruber, R. M. Key, K. Lee, J. L. Bullister, R. Wanninkhof, C. S. Wong, D. W. R. Wallace, B. Tilbrook, F. J. Millero, T.-H. Peng, A. Kozyr, T. Ono, and A. F. Rios. The oceanic sink for anthropogenic CO_2. *Science*, 305(5682):367–371, July 2004. doi:10.1126/science.1097403.

M. A. White, F. Hoffman, W. W. Hargrove, and R. R. Nemani. A global framework for monitoring phenological responses to climate change. *Geophys. Res. Lett.*, 32(4):L04705, Feb. 2005. doi:10.1029/2004GL021961.

Extra Slides

The USDA Forest Service, NASA Stennis Space Center, DOE Oak Ridge National Laboratory, and DOI Eros Data Center have created a system to monitor threats to U.S. forests and wildlands:

- Tier 1: Strategic — The *ForWarn* system that routinely monitors wide areas at coarser resolution, repeated frequently — a *change detection system* to produce alerts or warnings for particular locations may be of interest
- Tier 2: Tactical — Finer resolution airborne overflights and ground inspections of areas of potential interest — *Aerial Detection Survey (ADS)* monitoring to determine if such warnings become alarms

Tier 2 was in place and managed by the USDA Forest Service, but Tier 1 was needed to optimally direct its labor-intensive efforts and discover new threats sooner.

- To detect vegetation disturbances, the current NDVI measurement is compared with the normal, expected baseline for the same location.
- Substantial decreases from the baseline represent potential disturbances.
- Any increases over the baseline may represent vegetation recovery.
- Maximum, mean, or median NDVI may provide a suitable baseline value.

June 10–23, 2009, NDVI is loaded into blue and green; maximum NDVI from 2001–2006 is loaded into red (Hargrove et al., 2009).

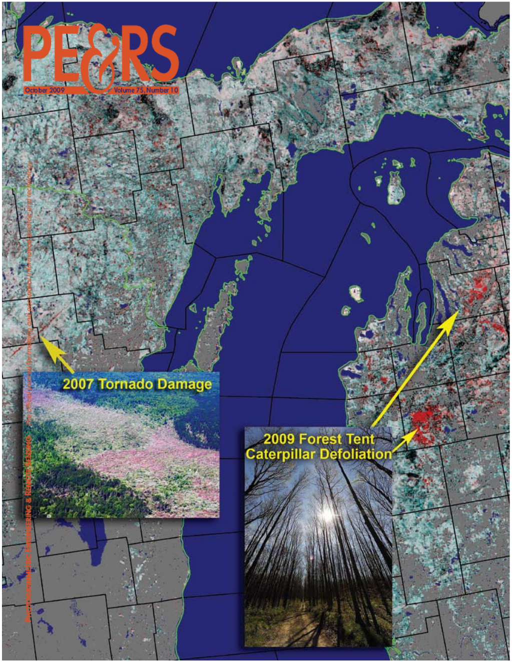

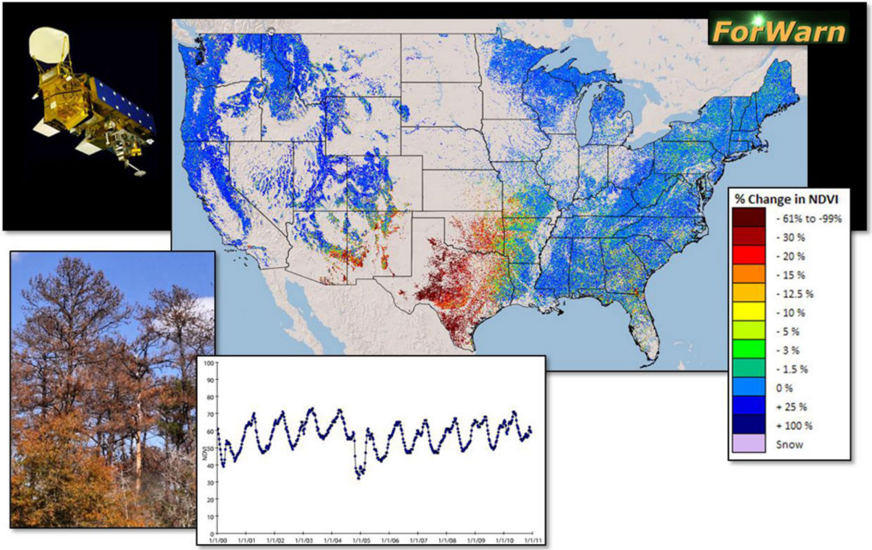

ForWarn is a forest change recognition and tracking system that uses high-frequency, moderate resolution satellite data to provide near real-time forest change maps for the continental United States that are updated every eight days. Maps and data products are available in the **Forest Change Assessment Viewer** at
`http://forwarn.forestthreats.org/fcav2/`

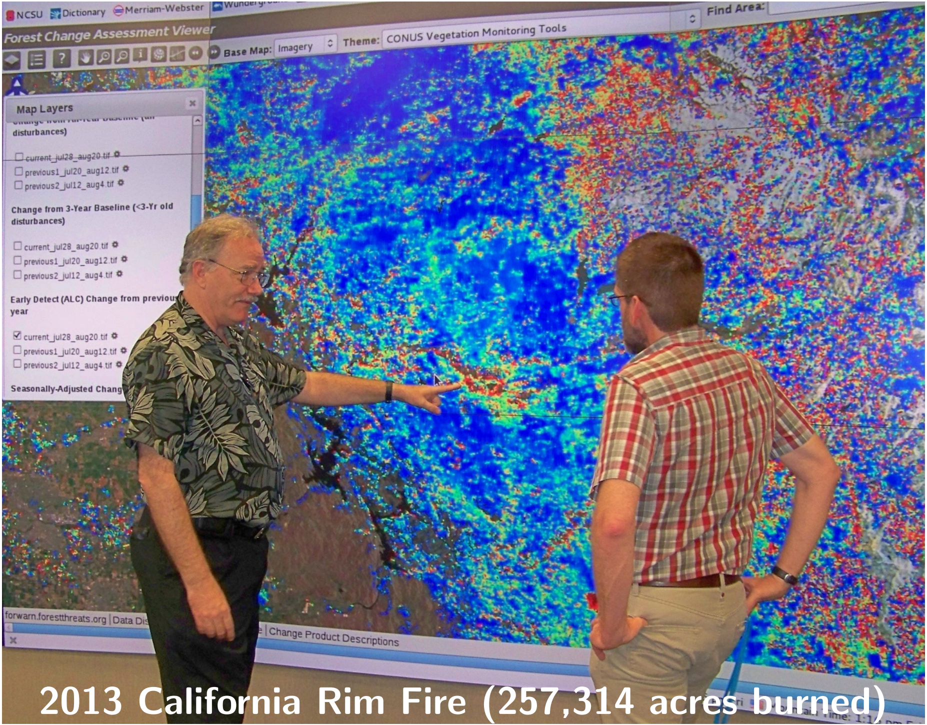

2013 California Rim Fire (257,314 acres burned)

Clustering MODIS NDVI to Produce Phenoregions

- Hoffman and Hargrove previously used *k*-means clustering to detect brine scars from hyperspectral data (Hoffman, 2004) and to classify phenologies from monthly climatology and 17 years of 8 km NDVI from AVHRR (White et al., 2005).
- This data mining approach requires high performance computing to analyze the entire body of the high resolution MODIS NDVI record for the continental U.S.
- $>$101B NDVI values, consisting of $\sim$146.4M cells for the CONUS at 250 m resolution with 46 maps per year for 15 years (2000–2014), analyzed using *k*-means clustering.
- The annual traces of NDVI for every year and map cell are combined into one 395 GB single-precision binary data set of 46-dimensional observation vectors.
- Clustering yields 15 phenoregion maps in which each cell is classified into one of *k* phenoclasses that represent prototype annual NDVI traces.

50 Phenoregions for year 2012 (Random Colors)

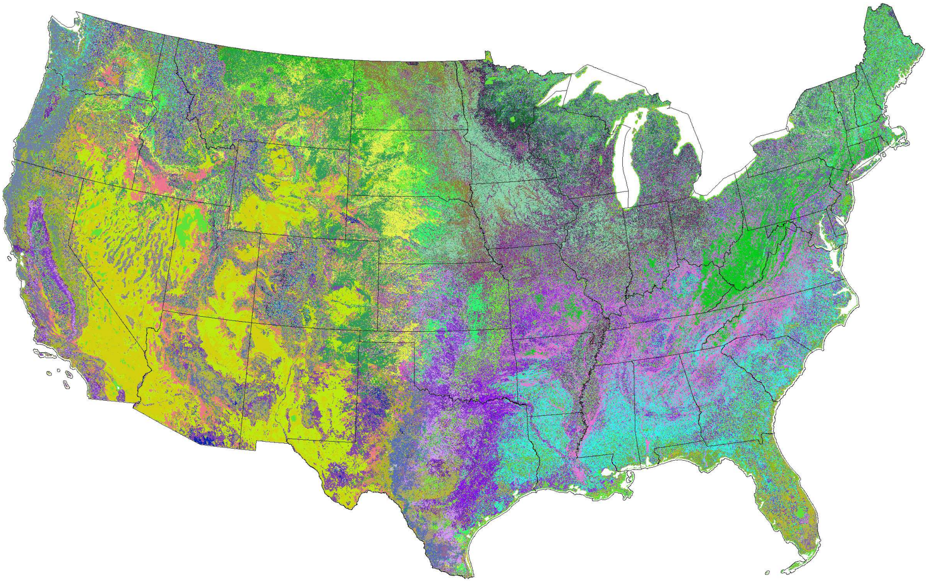

50 Phenoregion Prototypes (Random Colors)

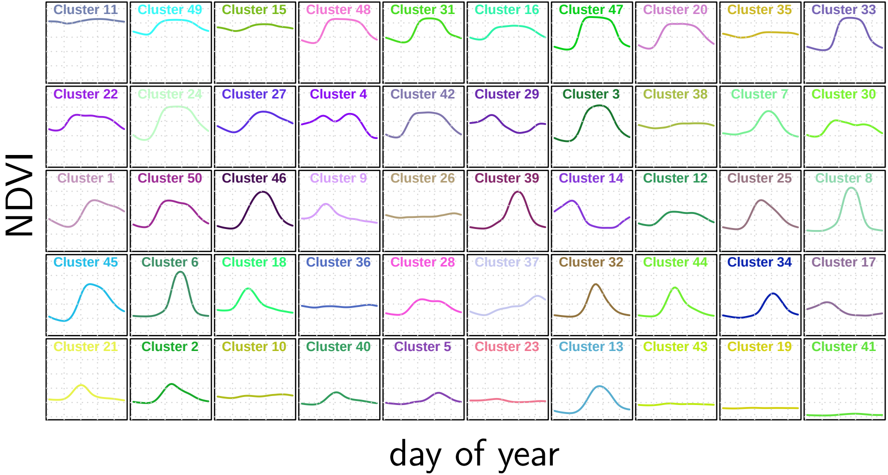

50 Phenoregions Persistence

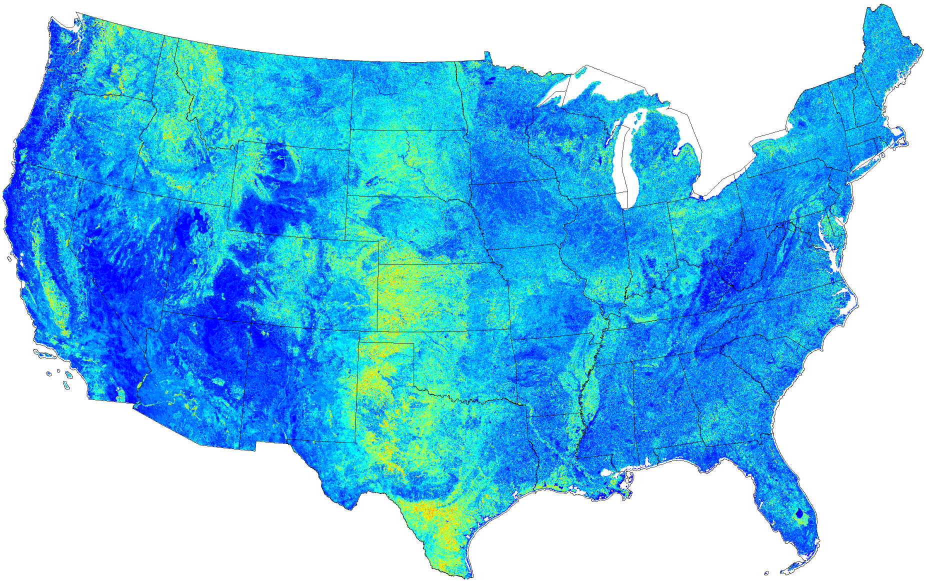

50 Phenoregions Mode (Random Colors)

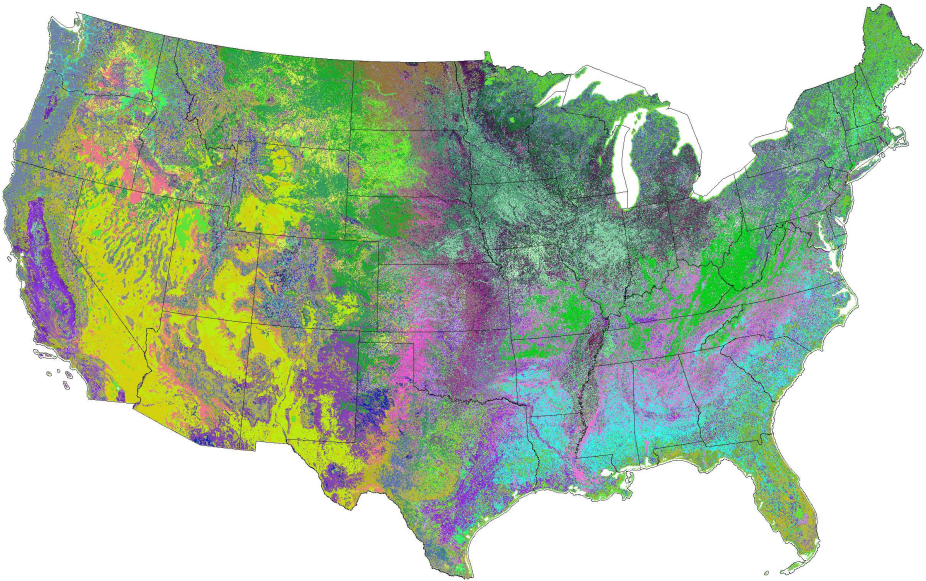

50 Phenoregions Max Mode (Random Colors)

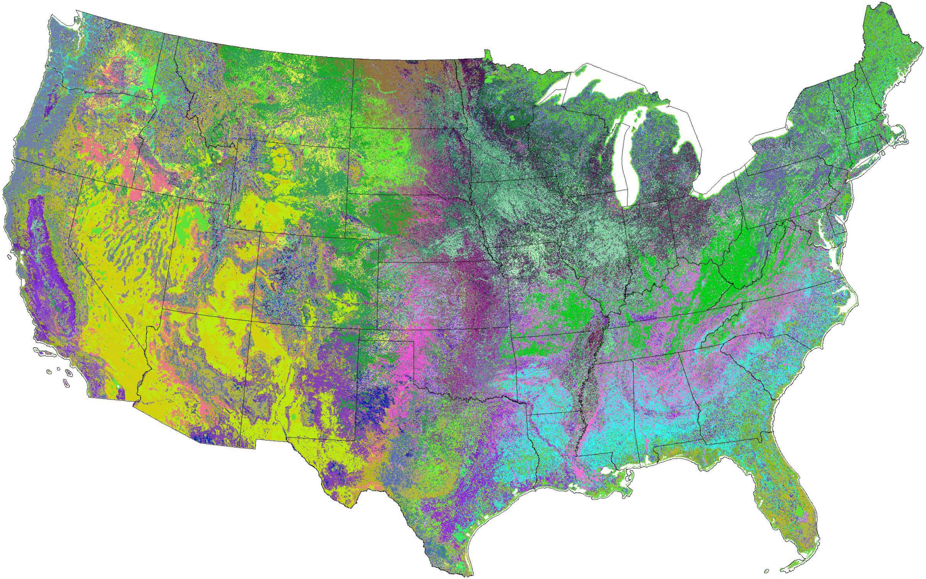

50 Phenoregions Max Mode (Similarity Colors)

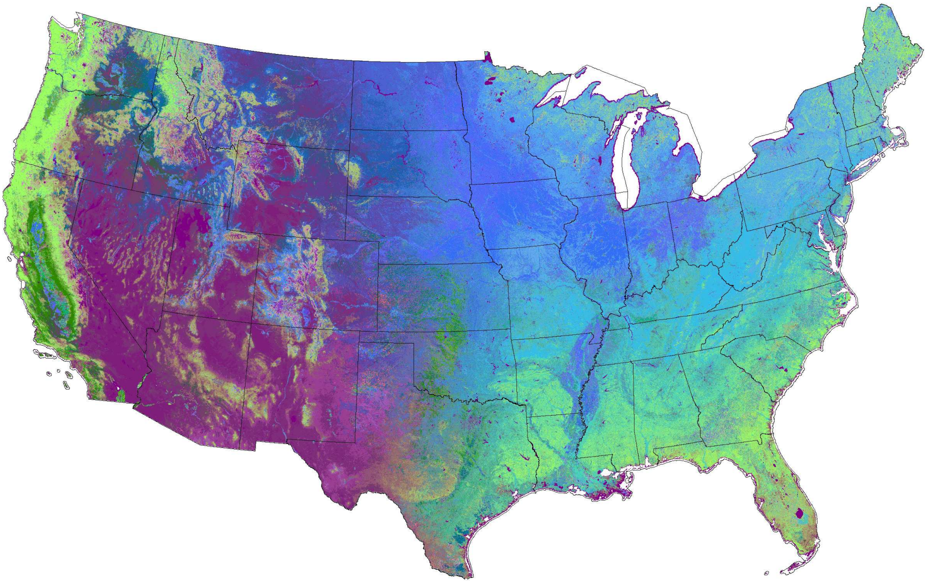

50 Phenoregions Max Mode (Similarity Colors Legend)

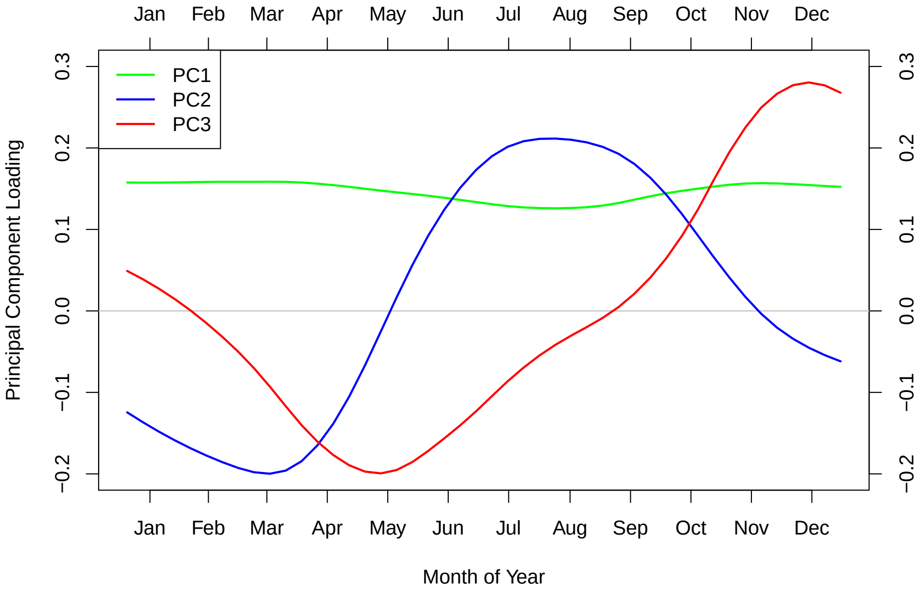

Phenoregions Clearinghouse

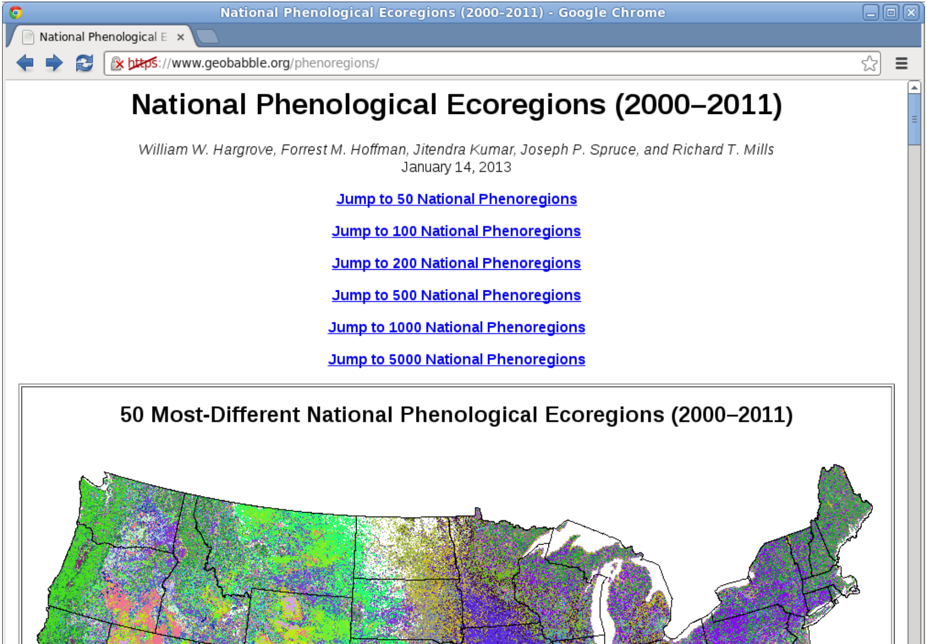

Emergent Constraint Developed from CMIP5 ESMs

An emergent constraint based on carbon inventories was applied to future atmospheric CO_2 projections from CMIP5 ESMs.

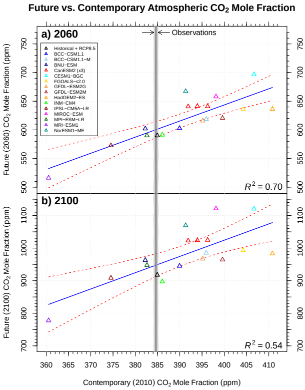

- Much of the model-to-model variation in projected CO_2 during the 21st century is tied to biases that existed during observational era.
- Model differences in the representation of concetration–carbon feedbacks and other slowly changing carbon cycle processes appear to be the primary driver of this variability.
- Range of temperature increases at 2100 slightly reduced, from $5.1 \pm 2.2°C$ for the full ensemble, to $5.0 \pm 1.9°C$ after applying the emergent constraint.

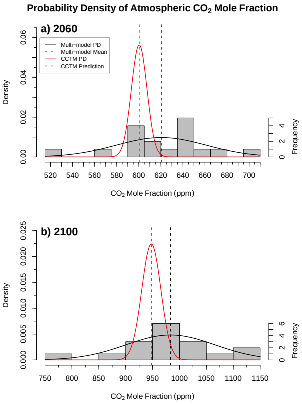

Best estimate using Mauna Loa CO_2

At 2060: 600 ± 14 ppm, 21 ppm below the multi-model mean

At 2100: 947 ± 35 ppm, 32 ppm below the multi-model mean

Hoffman, Forrest M., James T. Randerson, Vivek K. Arora, Qing Bao, Patricia Cadule, Duoying Ji, Chris D. Jones, Michio Kawamiya, Samar Khatiwala, Keith Lindsay, Atsushi Obata, Elena Shevliakova, Katharina D. Six, Jerry F. Tjiputra, Evgeny M. Volodin, and Tongwen Wu. February 2014. "Causes and Implications of Persistent Atmospheric Carbon Dioxide Biases in Earth System Models." *J. Geophys. Res. Biogeosci.*, 119(2):141–162. doi:10.1002/2013JG002381. *Most downloaded JGR-B paper for February 2014.*

Model inventory comparison with Sabine et al. (2004)

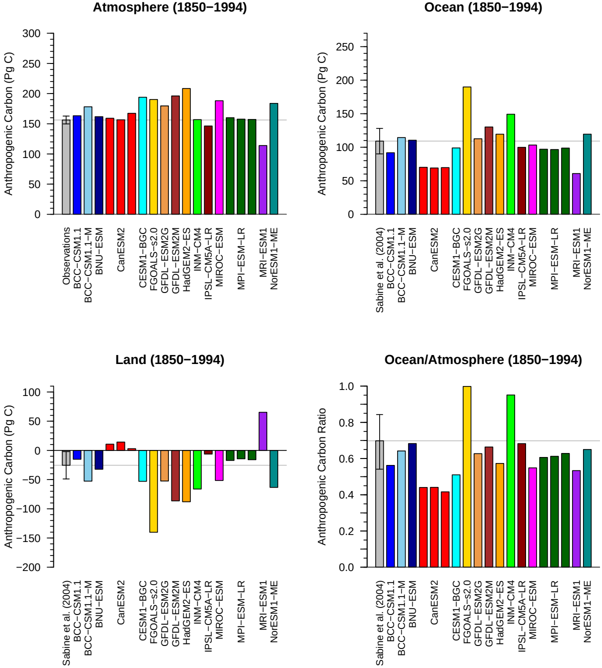

Implications for CO_2, Radiative Forcing, and Temperature

Model	CO_2 Mole Fraction (ppm)			Radiative Forcing ($W\,m^{-2}$)			Cumulative ΔT (°C)			ΔT Bias (°C)		
	2010	2060	2100	2010	2060	2100	2010	2060	2100	2010	2060	2100
BCC-CSM1.1	390	603	945	1.70	4.03	6.43	0.97	2.39	4.02	0.03	0.02	−0.01
BCC-CSM1.1-M	396	619	985	1.78	4.16	6.65	1.04	2.49	4.16	0.10	0.12	0.13
BNU-ESM	382	602	963	1.59	4.02	6.53	0.90	2.33	4.07	−0.04	−0.04	0.04
CanESM2 r1	394	641	1024	1.75	4.36	6.86	0.98	2.58	4.30	0.04	0.21	0.27
CanESM2 r2	392	641	1023	1.72	4.35	6.85	0.98	2.57	4.30	0.04	0.20	0.27
CanESM2 r3	396	641	1025	1.78	4.35	6.87	1.01	2.58	4.30	0.07	0.21	0.27
CESM1-BGC	407	697	1121	1.92	4.80	7.34	1.12	2.85	4.64	0.18	0.48	0.61
FGOALS-s2.0	404	636	993	1.89	4.31	6.70	1.09	2.57	4.23	0.15	0.20	0.20
GFDL-ESM2G	395	616	967	1.77	4.14	6.56	1.04	2.49	4.12	0.10	0.12	0.09
GFDL-ESM2M	400	621	964	1.83	4.18	6.54	1.09	2.52	4.13	0.15	0.15	0.10
HadGEM2-ES	411	636	983	1.98	4.31	6.64	1.18	2.60	4.20	0.24	0.23	0.17
INM-CM4	386	591	897	1.64	3.92	6.15	0.92	2.36	3.86	−0.02	−0.01	−0.17
IPSL-CM5A-LR	375	573	908	1.48	3.75	6.22	0.86	2.21	3.87	−0.08	−0.16	−0.16
MIROC-ESM	398	658	1121	1.81	4.50	7.35	1.06	2.67	4.58	0.12	0.30	0.55
MPI-ESM-LR r1	383	590	948	1.60	3.91	6.45	0.95	2.31	4.03	0.01	−0.06	0.00
MRI-ESM1	361	516	778	1.28	3.20	5.39	0.74	1.89	3.33	−0.20	−0.48	−0.70
NorESM1-ME	391	667	1070	1.72	4.57	7.09	0.98	2.68	4.46	0.04	0.31	0.43
Multi-model Mean	392	621	980	1.72	4.18	6.63	1.00	2.48	4.17	0.06	0.11	0.14
CCTM Estimate	385	600	948	1.62	4.01	6.45	0.94	2.37	4.03	—	—	—
Historical + RCP 8.5	385	590	917	1.63	3.91	6.27	0.94	2.32	3.93	0.00	−0.05	−0.10